ISSN 1023-1935, Russian Journal of Electrochemistry, 2012, Vol. 48, No. 3, pp. 259–270. © Pleiades Publishing, Ltd., 2012.
Published in Russian in Elektrokhimiya, 2012, Vol. 48, No. 3, pp. 285–298.

An Influence of Pretreatment Conditions on Surface Structure and Reactivity of Pt(100) Towards CO Oxidation Reaction[1]

A. V. Rudnev[a, b, z] and T. Wandlowski[b, z]

[a] *Frumkin Institute of Physical Chemistry and Electrochemistry, Russian Academy of Sciences, Leninskii pr. 31, Moscow, 119071 Russia*

[b] *Department of Chemistry and Biochemistry, University of Bern, Freiestrasse 3, CH-3012 Bern, Switzerland*

Received May 3, 2011

Abstract—We present a combined electrochemical and in situ STM study of the surface structure of Pt(100) single crystal electrodes in dependence on the cooling atmosphere after flame annealing. The following cooling conditions were applied: Ar/H_2 and Ar/CO mixtures (reductive atmosphere), argon (inert gas) and air (oxidative atmosphere). Surface characterization by in-situ STM allows deriving direct correlations between surface structure and macroscopic electrochemical behavior of the respective platinum electrodes. We investigated the influence of defect type and density as well as long range surface order on the kinetics of the CO electro-oxidation reaction. The defect-rich Pt(100) electrodes as cooled in air or Ar, and followed by immersion in the hydrogen adsorption region display higher activities as compared to the rather smooth Pt(100)-(1×1) electrode cooled in an Ar/H_2-atmosphere.

Keywords: single crystal, platinum, cyclic voltammetry, scanning tunneling microscopy, Pt(100), carbon monoxide

DOI: 10.1134/S1023193512030123

1. INTRODUCTION

The development of novel electrocatalytic materials to explore molecular details and reaction pathways represents one of the long standing goals in surface electrochemistry [1]. Studies with model catalyst, such as single crystal electrodes and/or nanoclusters of controlled morphology, composition and shape provide knowledge on relationships between atomic-level surface structure and catalytic properties [1–5]. This approach provides also an important guidance for the development and optimization of commercial catalysts [6, 7]. Platinum and its various alloy components represent one of the main families of electrocatalysts with paramount importance [1, 6, 8–10]. In consequence, low index and stepped platinum single crystals have been employed as model catalysts in a wide range of applications, e.g. for CO oxidation [11–14], the oxidation of small organic molecules such as formic acid and methanol [3, 9, 15, 16], the reduction of NO_3^- [17–19] etc. Various experimental strategies have been developed to modify and to tune the electrocatalytic properties of platinum surfaces [2, 5, 20]. Examples are underpotential (UPD) and overpotential deposition (OPD) of thin films of foreign metals, surface alloying and dealloying, introducing of controlled defect sites etc. [2, 10, 21–31]. Despite the considerable progress in studies of electrocatalytic interfacial reactions, there is a major lack in identifying and understanding, at an atomistic respective molecular level, the nature of "active sites" for many interfaciai reactions, even for reactions as widely studied as CO electro-oxidation [32]. State-of-the-art approaches combine classical electrochemical techniques, such as cyclic voltammetry or chronoamperometry with surface-science-based structure sensitive in-situ methods and quantum chemical model calculations to advance this field further [1, 23, 29, 33–38]. This knowledge is of great importance for the development of improved electrocatalysts for a wide range of industrial applications, in particular in areas such as energy or mobility [2].

In the present work we focus on the preparation and characterization Pt(100), one of the three low-index phases of platinum. Since the seminal work of Clavilier [39, 40] on the flame-annealing and quenching method to prepare single crystal electrodes, the characterization and understanding of the Pt(100)/aqueous electrolyte interface and its electrocatalytic properties advanced significantly [1, 5, 41–47]. Clavilier's method represents a convenient alternative to the rather elaborate sputtering and annealing strategies developed in ultra-high vacuum for the preparation of clean and well-ordered Pt(100) surfaces [48–54]. However, already Scortichi et al. [44, 45] pointed out on the gen-

[1] The article is published in the original.

[z] Corresponding authors: rudnev@dcb.unibe.ch (A.V. Rudnev), thomas.wandlowski@dcb.unibe.ch (T. Wandlowski).

eration of lattice strain and surface defects as a consequence of the rapid cooling and subsequent quenching in aqueous solution. Several groups introduced an intermediate slow cooling step, typically in hydrogen, in an argon/hydrogen atmosphere [55–57] or in iodine vapor being subsequently replaced by a CO monolayer in solution [58].

Despite the large amount of work published for platinum single crystal electrodes since the pioneering reports of Clavilier et al. [39, 40], there are still many open questions and controversies regarding the influence of cooling conditions on surface morphology and, as a consequence, on the electrocatalytic activity of Pt(100) electrodes. To the best of our knowledge, there exist only a few reports exploring the effect of a different cooling atmosphere on the surface morphology of Pt(100) combining structure-sensitive characterization techniques with voltammetric experiments [37, 59–62].

In the following we present a systematic study on the influence of four different cooling atmospheres (argon/hydrogen, argon/CO, argon and air) on the surface morphology of Pt(100). The electrodes, as prepared by flame-annealing, and different cooling protocols, are characterized by in-situ STM in combination with cyclic voltammetry. The role of surface defects will be illustrated for the CO electro-oxidation as a particular important model reaction. The experimental observations of the present study will be carefully compared with literature data aiming to resolve some of the still existing controversies and motivating detailed modeling studies on structure and stability of Pt(100) surfaces under electrochemical conditions.

2. EXPERIMENTAL

2.1. Electrochemical Measurements

We employed in all electrochemical experiments Clavilier-type bead single crystal electrodes in a hanging meniscus configuration [39, 40, 46, 63]. The beads were prepared by zone melting in an electron beam under ultrahigh vacuum conditions, preoriented with a He–Ne laser, and subsequently mechanically polished down to a hemispherical shape to increase the area (typically 0.03–0.07 cm^2) of the desired surface orientation exposed to electrolyte contact [64]. X-ray diffraction revealed an orientation to be better than 0.2° with respect to the nominal (100) plane.

Before each experiment, the Pt(100) electrode was annealed in a butane flame for 1 min to avoid any contamination and to obtain a well-ordered reconstructed surface structure. The hot electrode was quickly transferred into a closed flask filled with a mixture of Ar/H_2 ($Ar : H_2 = 4 : 1$), Ar/CO ($Ar : CO = 5 : 1$) or air, and allowed to cool down to room temperature. Cooling in pure Ar was directly performed in the electrochemical cell. Flow and composition of the gases in the flask and the cell were adjusted to ensure a slow cooling rate. The electrodes cooled in an Ar/H_2 mixture were immersed into deaerated Milli-Q water, which was saturated with H_2, and transferred with a protecting droplet of water adhering to the polished surface into the electrochemical cell. The electrodes cooled in CO-containing atmosphere and in air were transferred without a protecting water droplet.

The electrochemical measurements were conducted in a three compartment all-glass cell with a platinum or gold coil as auxiliary electrodes and a trapped reversible hydrogen reference electrode (RHE) in 0.5 M H_2SO_4. All potentials in this paper are referred to the RHE scale. The cell was equipped with an additional inlet for dosing CO (Carbagas 99.997).

The electrolytes were prepared from H_2SO_4 (suprapure, Merck) and Milli-Q water (18.2 MOhm, estimated total organic content 2–3 ppb). High-purity Ar (Carbagas 99.999) was employed to deaerate the solutions, and Ar was also passed above the solutions during the experiments. The freshly prepared electrodes were brought in contact with the electrolyte in a hanging meniscus configuration at $E = 0.150$ V, i.e. in the hydrogen adsorption region. The scan rate was 5 or 50 mV/s. The electrochemical measurements were carried out with an Autolab PGSTAT30.

2.2. Scanning Tunneling Microscopy (STM) Measurements

The STM measurements were carried out with a PicoSPM system (Molecular Imaging) in a sealed, argon-filled chamber. The working electrode was a Pt(100) hemispherical bead attached to a polycrystalline platinum sheet. The bead electrode was prepared according to a procedure outlined above. The area of the polished bead amounts to ~0.12 cm^2. The STM liquid cell was mounted on top of the Pt electrode for in situ and ex situ STM experiments. After flame-annealing, the platinum electrode was cooled down in the desired atmosphere (see above) and subsequently immersed into acidic 0.2 M $NaNO_2$ (>99.99%, Sigma Aldrich) solution for 1 min to cover the surface with adsorbed NO. The NO-protected electrode was rinsed thoroughly with ultrapure water to remove residues of the nitrite solution, and then mounted into the STM cell. NO was quantitatively reduced to ammonium cations upon immersion of the electrode at 0.150 V [65]. In situ STM experiments were performed with electrochemically etched tungsten tips (0.25 mm diameter) coated with polyethylene. A platinum wire and a palladium wire, charged with hydrogen, served as counter and reference electrodes, respectively. Contact of the working electrode with the electrolyte was established under strict potential control.

Ex situ STM experiments were carried out with electrochemically etched Pt/Ir (70/30) tips. For image processing we used the WSxM software [66].

3. RESULTS AND DISCUSSION

3.1. Morphological Study

Figures 1a and 1b show cyclic voltammograms (CVs) of a Pt(100) electrode in 0.5 M H_2SO_4 in the double layer region $0.050 \le E \le 0.600$ V, scan rate 50 mV s^{-1}, as cooled down, in four different atmospheres after flame annealing. The CVs show distinct changes in the appearance of the two pairs of characteristic current peaks *P*1 at ~0.380 V and *P*2 at ~0.280 V, as well as in the potential region below 0.200 V, depending on the chosen preparation of the electrode. The characteristic peaks correlate with the nature and density of the adsorption sites on the surface, in particular the (100) terraces, (111) and (110) steps as well as kinks (Fig. 1c and [20]). In the potential range investigated hydrogen underpotential deposition (UPD) takes place simultaneously with (bi)sulfate desorption. This reaction is strongly sensitive to the Pt(*hkl*) substrate surface structure. Clavilier et al. [67–69] assigned the peak *P*1 and the shoulder at *P*2, as observed for a Pt(100) cooled in an Ar/H_2 atmosphere, to the hydrogen adsorption coupled with the (bi)sulfate desorption (for the cathodic scan) on (100) terrace sites and on terrace sites close to steps, respectively. Hydrogen adsorption at (111) and (110) step sites was attributed to the rather featureless current response below 0.200 V, just before the onset of hydrogen evolution. However, Markovic et al. [57] and Watanabe et al. [70] assigned the signal at 0.280 V to the H adsorption/sulfate desorption at (111) step sites. This assignment is supported by a systematic voltammetry study of the Alicante group with stepped Pt[n(100) × (111)] electrodes in H_2SO_4 (see Fig. 1 in [28]). Sulfate ions are adsorbed stronger at steps and kinks than on terraces and block these sites for H adsorption. More negative potentials are needed to desorb anions and to vacate defect sites for hydrogen adsorption. Higher currents at potentials below 0.200 V could be related to the adsorption/desorption of H and anions at kink and (110) step sites (see the scheme in Fig. 1c). This hypothesis is supported by additional voltammetric studies of the Alicante group with stepped Pt[n(100) × (110)] electrodes in H_2SO_4 [71]. The currents at $E < 0.200$ V increase with step density. At the same time the peak at ~0.280 V also appears and grows with increasing step density. However, its magnitude is much lower as compared to stepped Pt[n(100) × (110)] single crystals. This observation could be tentatively attributed to a rearrangement of Pt atoms at (110) step sites into short (111) step sites [72].

In-situ STM investigations on the surface morphology of these sites upon polarization in combination with quantum chemical model calculations on the competitive adsorption of H and sulfate species on the various Pt(100) surface sites under conditions of an applied electrochemical potential are essential to gain a more detailed atomistic understanding on the com-

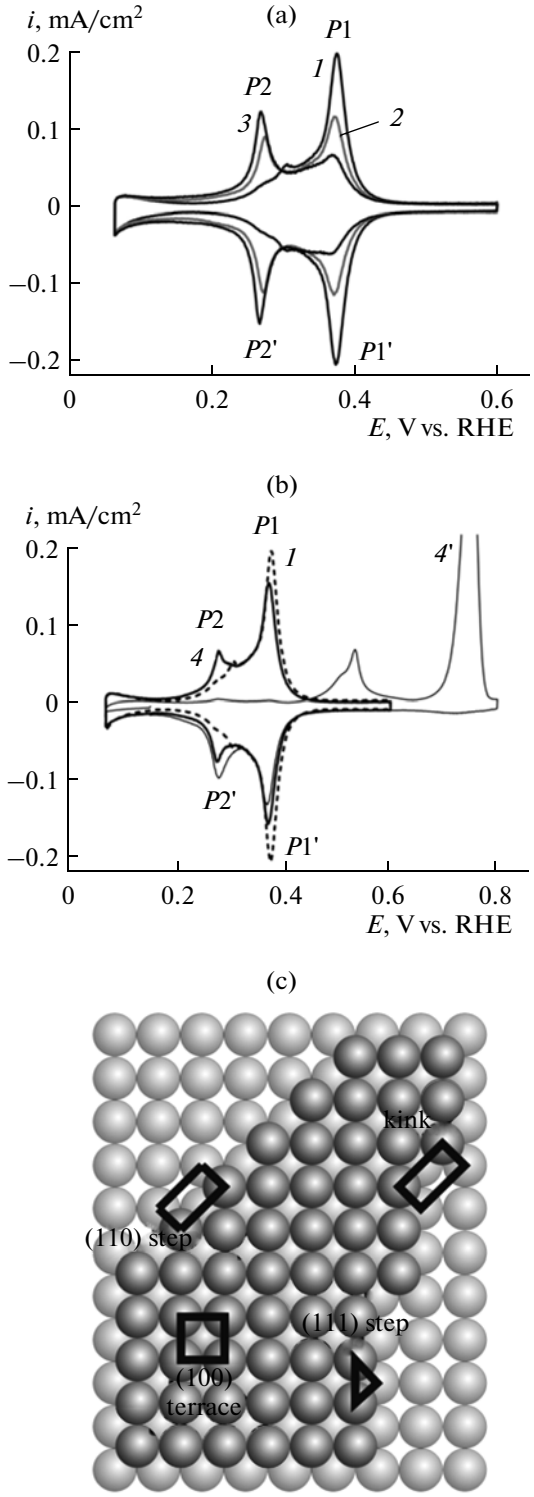

Fig. 1. (a, b) Cyclic voltammograms (CVs) of Pt(100)-(1 × 1) in 0.5 M H_2SO_4 for flame-annealed electrodes cooled down in different atmospheres: (*1*) Ar/H_2, (*2*) Ar, (*3*) air, (*4* and *4*') Ar/CO. Curve *4* was recorded after CO stripping during the CV denoted *4*'. The scan rate is 50 mV/s. (c) Schematic top view of Pt(100)-(1 × 1) surface containing different adsorption sites.

plex behavior of the Pt(100) surface in contact with H_2SO_4.

In the following we compare voltammetric data and in-situ STM experiments of Pt(100) electrodes prepared under four conditions, giving rise to distinctly different surface-structure related responses.

Cooling of the flame-annealed Pt(100) electrode in an Ar/H_2 mixture leads to a high and rather narrow current peak *P*1 at 0.380 V, a shoulder at *P*2 ~ 0.280 V, and a small current plateau at $E < 0.200$ V in the entire double layer region as observed during the cathodic as well as anodic potential scan (curve *1* in Figs. 1a, 1b, and as an example [73]). Cooling in an Ar/CO mixture (5 : 1) leads after oxidative stripping of CO upon potential excursion up to 0.800 V, to a pronounced current peak *P*1 at 0.380 V (line *4* in Fig. 1b), which is slightly lower than the one observed for cooling in an Ar/H_2 mixture, and to the evolution of very small peak-like features *P*2 around 0.280 V. The latter may be caused by potential excursion up to 0.800 V, which induces surface defect sites [37, 74]. The voltammogram recorded after cooling in a pure Ar atmosphere and subsequent immersion of the electrode at 0.150 V shows upon cycling the potential two distinct current peaks at *P*1 ~ 0.380 V and *P*2 ~ 0.280 V, and a significant increase of the double layer current in $E < 0.200$ V (curve *2* in Fig. 1a). *P*1 is lower, and *P*2 is higher as compared to the voltammogram obtained after cooling in an Ar/H_2 mixture. Cooling in air (trace *3* in Fig. 1a) reduces *P*1 even further, and simultaneously the currents of *P*2 and the current in the region $E < 0.200$ V increase. These trends have been observed before (see [37, 46] and cites herein), but were never systematically compared on the basis of accompanying in-situ studies of the respective surface morphologies.

Figures 2a and 2b show typical in situ STM images of a Pt(100) surface as prepared by flame annealing followed by slow cooling in an Ar/H_2 stream (see also [75]). The surface exhibits long and wide terraces, which alternate with step-bunched regions. On terraces wider than 500 nm we also observed square-shaped Pt ad-islands of 0.21 nm height and 10 to 40 nm in *X*,*Y* dimensions (Fig. 2a, and the inset). All islands are aligned along [011] or one of the equivalent lattice directions. The relative orientation of the islands with respect to the step edges also indicates that the steps observed in Fig. 2a represent (111)-type steps. Furthermore, the island density is the largest in the center of the terrace, and decreases towards the edges. The island size is the smallest in the center of the terraces and increases considerably towards the edges. No islands are observed within up to 250 nm away from lower and upper step edges. Clearly, Pt adatoms are incorporated into steps and large islands during the cooling period. The presence of these aligned and square-shaped Pt islands also indicates that the Pt surface was reconstructed, and that the adsorption of hydrogen during the cooling period has transformed the initially reconstructed Pt(100)-hex-*R*0.7° surface into the unreconstructed Pt(100)-(1 × 1) plane. The lifting of the hex-reconstruction of Pt(100) upon hydrogen adsorption was observed in UHV studies by LEED and STM [60, 76, 77]. The close-packed reconstructed phase contains ca. 25% more surface atoms than the ideally terminated (1 × 1) squared lattice. Upon lifting of the reconstruction, the excess platinum adatoms form square-shaped islands or diffuse across terraces to be embedded into step edges if distances are sufficiently short. Number, density and size of the Pt ad-islands can be tuned by hydrogen concentration and immersion temperature of the hot Pt(100) crystal into the Ar/H_2 mixture. Increasing temperature and hydrogen content will significantly increase the Pt adatom mobility, which reduces the number of platinum islands, and, as a consequence, the defect density on Pt(100)-(1 × 1) terrace sites [60, 76–78]. However, one should be careful in applying this strategy after annealing in an open flame, but rather chose a closed tubing system such as described for the inductive annealing of Pd or Rh electrodes [3, 64]. We note that similar STM-images as those shown in Figs. 2a and 2b were also observed without NO protection/deprotection, demonstrating that the Pt(100) surface morphology is not modified during this intermediate transfer step.

Cooling the flame-annealed Pt(100) electrode in an Ar atmosphere retains the reconstructed Pt(100)-hex-*R*0.7° surface. This is supported by the works of Inukai et al. [60], Zei et al. [79], and Al-Akl et al. [59, 80]. Al-Akl et al. stated that the Pt(100)-hex-*R*0.7° surface is stable in the presence of specifically adsorbed (bi)sulfate but unstable upon exposure to electrosorbed hydrogen [59, 80]. Zei et al. even claimed, based on ex-situ LEED and RHEED transfer experiments that the Pt(100)-hex-*R*0.7° electrode surface is stable in the entire potential region negative of the onset of surface oxidation [81]. The in-situ STM images obtained in our experiments in the absence as well as in the presence of a NO-protecting layer, and after immersion of the Pt electrode in the hydrogen adsorption region at 0.150 V do not support this statement. The Pt surface appears to be unreconstructed surface (Figs. 2c and 2d). We used two different protocols for Ar-cooled Pt(100) electrodes: (1) the cooled electrode was contacted in an electrochemical cell with 0.1 M H_2SO_4 at 0.150 V for 10 min, and subsequently transferred to the STM-cell with a droplet of electrolyte, and (2) using the NO protection/deprotection procedure described in the experimental part, without preliminary exposure to the electrolyte. We observed the same surface morphology in both cases: few wide terraces are separated by extended, highly facetted step regions with edges representing (110) and (111) step sites (Figs. 2c, 2d, and the inset in 2d). This pattern differs from data reported by Inukai et al. from UHV transfer experiments in 1 mM H_2SO_4 [60], who observed numerous islands up to 40 nm long and 10 nm wide after lifting of the reconstruction. Proba-

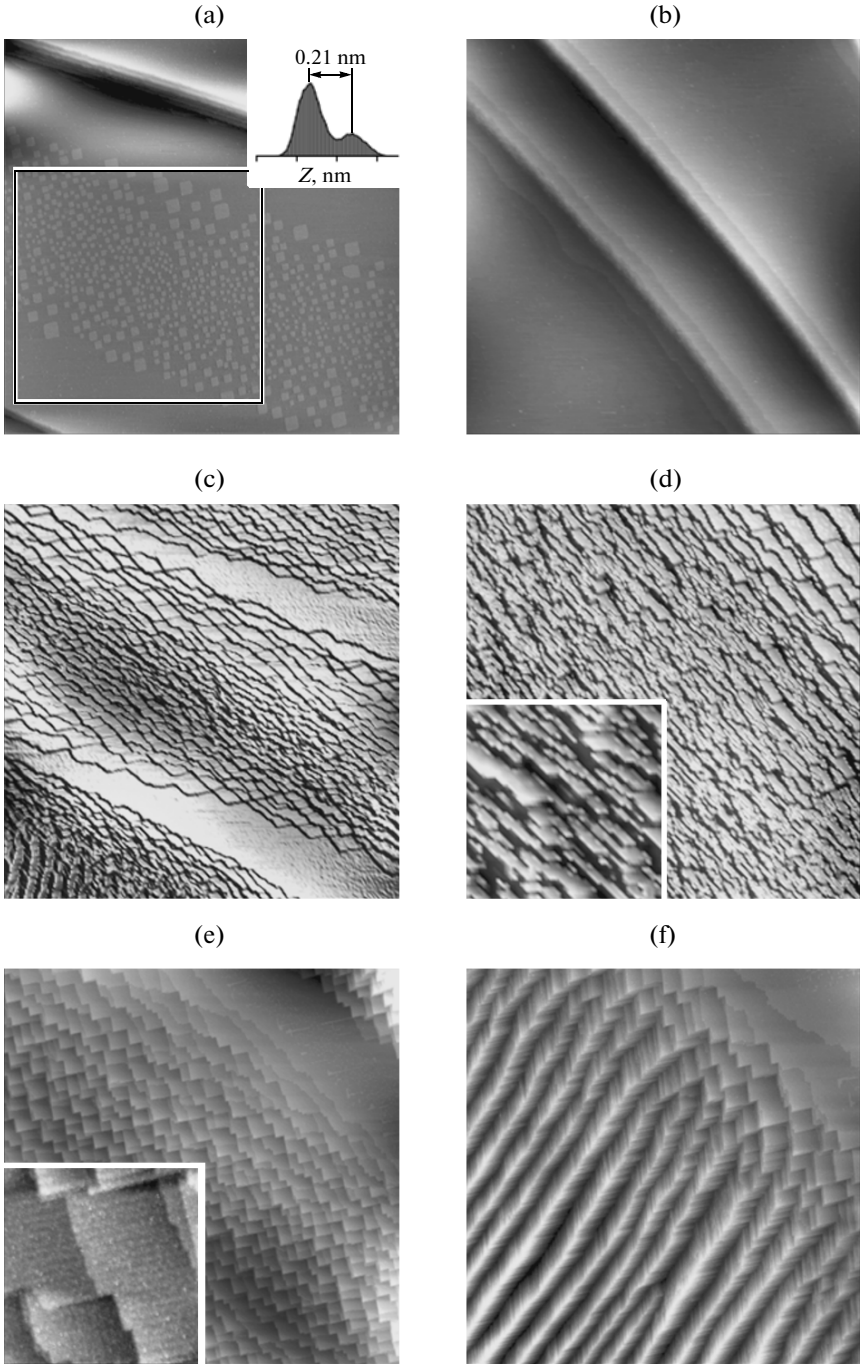

Fig. 2. In situ STM images of Pt(100)-(1 × 1) surfaces obtained in 0.1 M H_2SO_4 at $E = 0.100$ V. The cooling atmospheres were (a, b) Ar/H_2, (c, d) Ar and (e, f) air. The image areas are (a, c, e) 1.0×1.0 μm^2, (b, d, f) 0.5×0.5 μm^2. The images (c, d) are presented in a quasi-3D view. The inset in panel (a) represents the height distribution histogram of the selected square area: the distance between peaks corresponds to the height difference between surface and ad-island layers. Enlarged scale STM images (80×80 nm^2) are plotted in panels (d) and (e) as insets. They show structure details of the respective surface morphologies. Further information is given in the text.

bly, these Pt ad-islands are not stable and undergo a restructuring during a longer exposure of the electrode in more concentrated sulfuric acid solution in the potential range of hydrogen adsorption.

The modified and defect-rich surface morphology is also represented by distinct changes of the voltammetric response in the finger print region of hydrogen adsorption/(bi)sulfate desorption. The height of the

Comparison of the parameters obtained from CVs and CO displacement experiment

Cooling atmosphere	E_{pztc}, V vs. RHE	$E_{pre\text{-}peak}$, V	E_{Ox}, V	Q_{dis}, mC/cm^2	Q_{Ox}, mC/cm^2	$\int_{0.15}^{0.85} (i/v)\,dE$, mC/cm^2	Q_{CO}^{net}, mC/cm^2	θ
Ar/H_2	0.382	0.664	0.786	0.181	0.451	0.285	0.347	0.83
Ar	0.365	0.527	0.762	0.172	0.432	0.288	0.316	0.76
Air	0.361	0.553	0.764	0.172	0.435	0.292	0.315	0.76

Note: E_{pztc}—potential of zero total charge calculated from Eq. (2); the overall position of E_{pdc} is estimated ±0.005 V,
$E_{pre\text{-}peak}$—potential of the pre-peak of CO oxidation in the CV in Figs. 3b and 3c,
E_{Ox}—potential of the CO oxidation in the CV as displayed in Figs. 3b and 3c,
Q_{dis}—charge density displaced at 0.15 V during the potentiostatic adsorption of CO,
Q_{Ox}—charge density integrated from the voltammogram of the CO-covered Pt(100) surface between 0.150 and 0.850 V,
$\int_{0.15}^{0.85} (i/v)\,dE$—charge density integrated from the voltammogram of the CO-free Pt(100) surface between 0.150 and 0.850 V,
Q_{CO}^{net}—true CO oxidation charge density calculated from Eq. (5),
θ—CO coverage calculated from Q_{CO}^{net} assuming two-electron process of CO oxidation.

terrace-related peak *P*1 decreases by 40% as compared to an Ar/H_2-based cooling protocol. *P*2 develops into a clear current peak of considerable magnitude, and also the current plateau at $E < 0.200$ V increases (curve *2* in Fig. 1a).

Cooling of the hot Pt(100) electrode in air leads to highly facetted surface regions separated by terraces up to 200 nm wide and several hundreds of nanometer long. The facets are composed of small, but mutually aligned terraces of 10 to 50 nm size, interspaced by step-bunching regions. These features are aligned along the main crystallographic directions of the squared Pt(100)-(1 × 1) surface lattice and have mainly 90° angles at terrace edges, which suggests the preference of the thermodynamically more stable (111) step sites. Higher resolution images, such as shown in the inset of Fig. 2e also indicate the presence of kink defects. This inset further demonstrates that all terraces as well as the larger facets are covered with parallel stripes aligned with the two crystallographic directions of the quadratic Pt(100)-(1 × 1) surface lattice. The stripes are separated by ~3.5 nm and are composed of small Pt ad-islands of 1 to 2 nm in diameter. These stripes were also observed in ex-situ STM images reported by the Alicante group [61, 62] and in a recent study by Kibler et al. [37]. We conclude at this stage that the exposure of the initially reconstructed Pt(100)-(hex)*R*0.7° surface to oxygen lifts the reconstruction, which leads to a rough, defect rich electrode surface [37, 59]. The corresponding cyclic voltammogram (curve *3* in Fig. 1a) is characterized by a small peak *P*1 at 0.372 V, a large peak *P*2 at 0.272 V, and a further increase in the plateau current at $E < 0.200$ V.

The comparison of the cyclic voltammograms and in-situ STM images of Pt(100) electrodes prepared according to different cooling protocols revealed that a reductive Ar/H_2 atmosphere leads to long-range ordered Pt(100)-(1 × 1) terraces with a rather small number of defect sites. Cooling in Ar/CO gives similar results. However, the number of (111) step sites appears to be higher as compared to the former treatment. Cooling in an inert argon atmosphere retains the Pt(100)-(hex)*R*0.7° reconstruction [59, 80]. However, contact with the electrolyte in the H-adsorption region lifts this phase, accompanied with the creation of a defect-rich surface. Cooling in an oxygen-containing atmosphere leads to the formation of a large number of surface defects, such as (111) and (110) step sites as well as kinks accompanied with the appearance of highly facetted surface areas. We also like to emphasize that the STM images shown in this chapter are representative data selected from several individual experiments and after sampling of more than 10 different areas on the electrode surface. We are confident that all patterns shown represent typical morphologies of the various Pt(100) surfaces employed in the macroscopic electrochemical experiments, where one samples over the entire electrode surface exposed to the electrolyte in hanging meniscus configuration.

3.2. Electro-Oxidation of Carbon Monoxide

In the following chapter we explore the distinct effects of the Pt(100)-(1 × 1) surface morphologies, as obtained by the various cooling protocols, on the CO adsorption and electro-oxidation as an archetype test reaction for structure sensitivity.

Charge displacement experiments in 0.5 M H_2SO_4 upon dosing CO at 0.150 V, i.e. in the potential region of hydrogen adsorption, yield positive current transients (Fig. 3a) as a result of:

$$Pt\text{-}H_{ad} + CO = Pt\text{-}CO_{ad} + H^+ + e. \qquad (1)$$

The charges Q_{dis} estimated by integration of the CO displacement transients (Fig. 3a) are given in table. We

note that the theoretical charge of a full monolayer ($\theta = 1$) of an adsorbate on Pt(100)-(1 × 1) being involved in a one-electron process is 0.209 mC/cm^2 [73]. The charge displacement experiments enable, after integration of the anodic half-cycle of the voltammograms, an estimation of the potentials of zero total charge E_{pztc} of the three Pt(100)-(1 × 1) surfaces in 0.5 M H_2SO_4 according to [47, 82]:

$$Q_M(E) = \int_{0.15}^{E} (i/v)dE - Q_{dis}(0.15\ V), \qquad (2)$$

with i and v are current density and sweep rate, Q_M representing the charge density of the CO-free surface and Q_{dis} (0.15 V) being the charge displaced by CO at 0.15 V. The following sequence of E_{pztc} is obtained: 0.361 (air) < 0.365 (Ar) < 0.382 V (Ar/H_2) (table). This trends correlates with the decreasing number of surface defects [83].

After the formation of a saturated CO adlayer on Pt(100)-(1 × 1), the extra amount of CO was completely removed from the cell by Ar purging through and above the solution. Removal of CO from the CO-saturated solution results in a partial reversible desorption of the CO adlayer leading to a thermodynamic equilibrium between adsorbed CO and CO-containing electrolyte. Lopez-Cudero et al. [84] have shown that the maximum coverage θ_{CO} in CO-free solutions on Pt(100) amounts to 0.79. Subsequently, the electrode potential was scanned with 5 mV s^{-1} from 0.150 to 0.065 V, to 0.850 V and back to 0.150 V. The three voltammetric scans for Pt(100)-(1 × 1) as cooled down in Ar/H_2 (solid line *1*), Ar (dashed line *2*), and air (dash-dotted line *3*) are plotted in Fig. 3b. Figure 3c displays a magnification of these voltammograms. Two CO stripping peaks are clearly resolved during the positive potential sweep. The peak at $E = 0.420$–0.700 V corresponds to CO oxidation in the so-called "pre-ignition potential region." It is assigned to the oxidation of CO molecules adsorbed at defect sites of the (100) surface and to a small amount of CO molecules adsorbed at near terrace sites capable for diffusing toward steps within the time interval of potential polarization [74, 84]. Figure 3c illustrates that the pre-oxidation peak on the defect-rich Pt(100)-(1 × 1) electrode cooled in Ar is more than 100 mV more negative than that for Pt(100) electrode cooled in an Ar/H_2 atmosphere (table). CO oxidation on a Pt(100) electrode cooled in air is slightly hindered as compared to the electrode prepared according to the Ar cooling protocol.

Markovic et al. [74, 85, 86] suggested that the oxidative removal of a fraction of CO_{ad} in the pre-ignition region of Pt(111) and Pt(100) is accompanied by a simultaneous relaxation of the remaining CO adlayer, which generates a new binding state labeled as "strongly adsorbed CO". Although the nature of adsorbed CO_{ad} appears to be different before and after the pre-ignition region, these authors [74] proposed

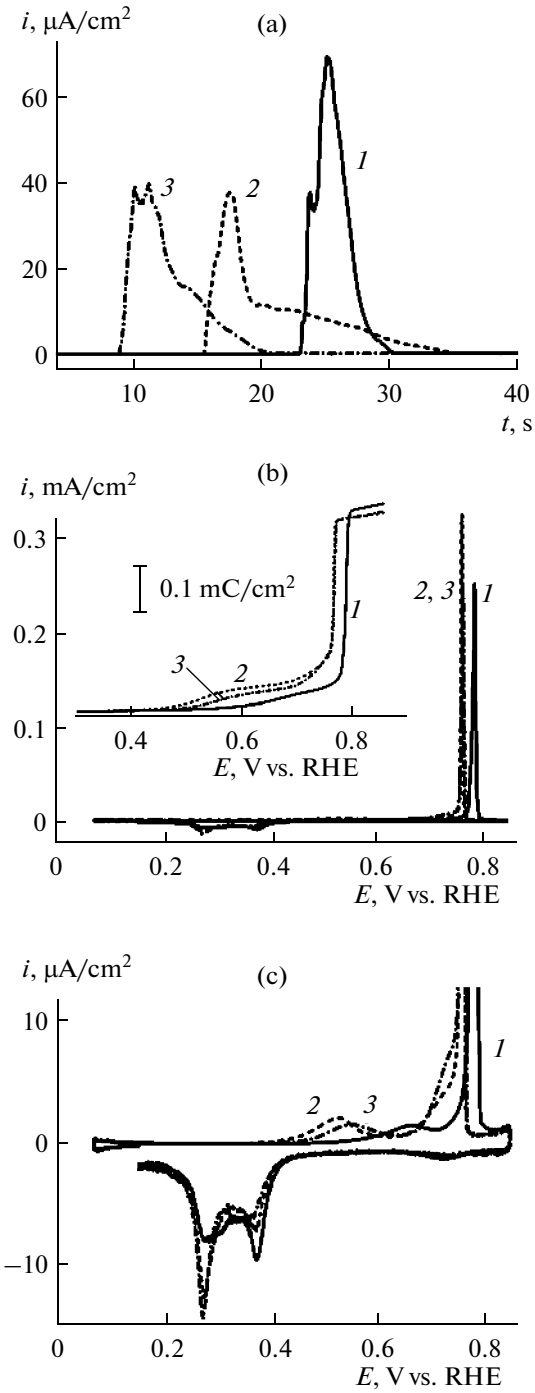

Fig. 3. (a) CO charge displacement transients for Pt(100)-(1 × 1) in 0.5 M H_2SO_4 at 0.150 V. (b) CVs for CO stripping on Pt(100) in CO-free 0.5 M H_2SO_4. (c) Expanded scale of (b). The scan rate is 5 mV/s. The inset in (b) shows the plot of the charge density of CO oxidation vs. potential in the range of 0.300–0.850 V. The Pt(100)-(1 × 1) electrode was flame annealed and cooled down in Ar/H_2 (4 : 1 mixture) (*1*, solid lines), Ar (*2*, dashed lines) and air (*3*, dash-dotted lines).

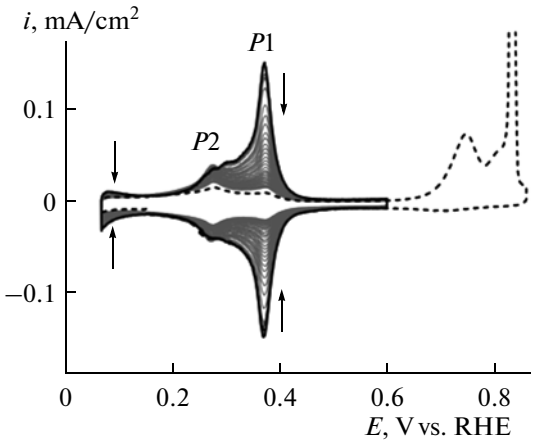

Fig. 4. Successive potential cycles recorded for Pt(100)-(1 × 1) as cooled in an Ar/H_2 mixture before (black solid line) and after (gray solid lines) the addition of a small amount of CO in the electrochemical cell. The black dashed line represents the last cycle, which was extended in the CO electro-oxidation region. The scan rate is 50 mV/s.

that the CO oxidation on Pt(100) is the same in both, the pre-ignition and ignition potential regions, and follows a "reactant-pair" mechanism originally proposed by Gilman [87]. This mechanism assumes a Langmuir–Hinshelwood type reaction between CO and a surface oxygen-containing species, adsorbed on adjacent sites, to form CO_2. The oxygen-containing species results from the oxidation of water at the electrode surface, and is usually suggested to be OH_{ad}, although the exact nature of this species is still unknown. The overall reaction scheme is:

$$H_2O + Pt = Pt\text{-}OH_{ad} + H^+ + e, \quad (3)$$

$$Pt\text{-}CO_{ad} + Pt\text{-}OH_{ad} = CO_2 + H^+ + e + 2Pt. \quad (4)$$

The main peak (in the ignition region) of CO oxidation on Pt(100) coincides with the range of reversibly adsorbed hydroxyl species ($0.700 < E < 0.800$ V) [74].

Recently, Markovic et al. [32] explored in a combined experimental and theoretical study the nature of the active sites for bulk CO electro-oxidation on the Pt(100) in the pre-ignition potential region. These authors suggested the undercoordinated atoms of ad-islands on Pt(100) as key reaction sites being superior in activity as compared to other surface sites such as terraces and steps. They also demonstrated that the interplay of OH_{ad} and CO_{ad} upon CO oxidation leads to the disappearance of these ad-islands followed by the formation of rather inactive step-like features [32]. Lebedeva et al. [88, 89] proposed, based on voltammetric and transient studies of CO electro-oxidation on stepped Pt electrodes with (111) terraces, that the active sites should be located at the inner corner of either (110) or (100) steps.

The main CO oxidative stripping peaks for the three types of Pt(100)-(1 × 1) electrodes investigated in this study or located at 0.786 V (Ar/H_2), 0.762 V (Ar) and 0.764 V (air), respectively (table). In other words, the main CO oxidation peak of the highly ordered Pt(100)-(1 × 1) surfaces develops at slightly more positive potentials as compared to the defect-rich air- and Ar-cooled electrodes (c.f. morphologies shown in Figs. 2c–2f). This small shift is remarkably different as compared to experiments on Pt(111) electrodes cooled in Ar/H_2 or in air [90]. In the latter case the presence of small amounts of defects leads to a negative shift in the position of the main CO electro-oxidation peak by several hundred mV [90, 91].

Integration of the CO-stripping voltammograms provides an estimation of the true CO oxidation charge density (Q_{CO}^{net}) [47, 84, 92]:

$$Q_{CO}^{net} = Q_{ox} + Q_{dis}(0.15\ V) - \int_{0.15}^{0.85} (i/v)dE, \quad (5)$$

where Q_{ox} is the experimentally determined integrated charge of the CO oxidation peak. The other two terms represent the double layer charge contribution due to anion adsorption on CO free sites (c.f. Eq. (2)). This process follows immediately the CO electro-oxidation step. The estimated charges Q_{CO}^{net} of defect-rich Pt(100)-(1 × 1) surfaces are rather similar and correspond to a CO coverage of ca. 0.76 (table). The estimated charge density and corresponding CO coverage are higher ($\theta = 0.83$) for electrodes prepared by Ar/H_2 cooling.

The integrated currents of the three positive-going potential sweeps (without double layer correction) can be considered as a "dynamic isotherm" of CO stripping (inset in Fig. 3b). The data show clearly that the two defect-rich electrode surfaces are more active with respect to CO oxidation than the highly ordered electrode surface, which was prepared by cooling in an Ar/H_2 atmosphere. This trend is particularly well resolved in the pre-ignition region. However, considering the different morphologies of the three types of Pt(100)-(1 × 1) electrode surfaces (Fig. 2), the rather moderate overall effect is somewhat surprising. Clearly, CO-electro-oxidation on Pt(100)-(1 × 1) is not favored by large and smooth (1 × 1) terraces. On the other hand, the above data also illustrate that the rate and activity of CO monolayer electro-oxidation is not necessarily determined by the total number of step sites.

In an attempt to learn more about the role of "active sites" for CO electro-oxidation, we carried out additional voltammetric experiments with sub-saturated CO-adlayers. Figure 4 shows successive potential cycles recorded for Pt(100)-(1 × 1) cooled in an Ar/H_2 mixture after the exposure to a small amount of CO in the electrochemical cell. This was accomplished by positioning the CO/Ar inlet above the solution and close to the electrode in hanging meniscus configuration at $E = 0.150$ V. The flow rate of the gas stream was very small. The CO dosing was stopped after 2 s, and only Ar was passed over the solution. The

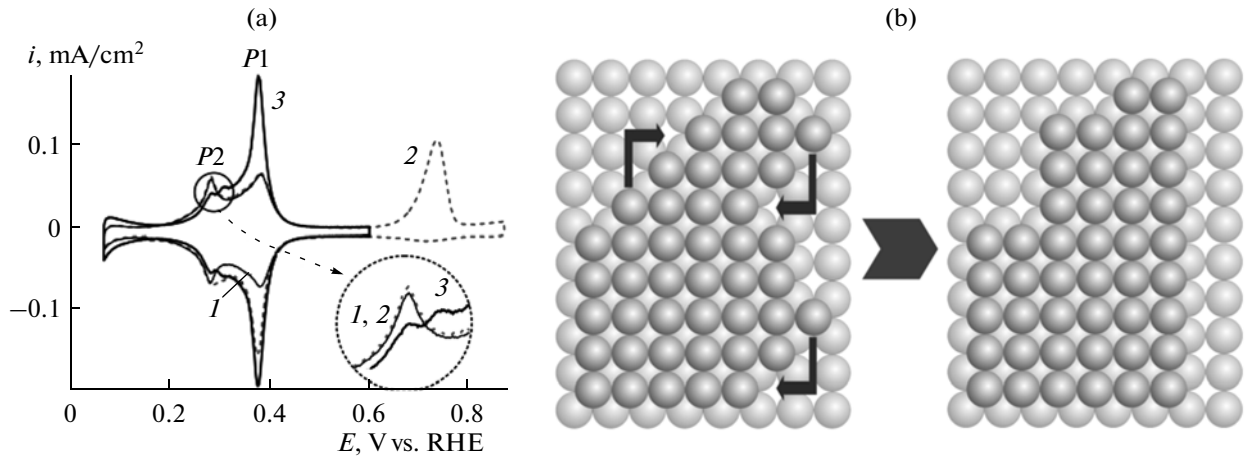

Fig. 5. (a) Comparison of CVs of a Pt(100)-(1 × 1) electrode for submonolayer coverage of CO: electrode partially blocked with CO in 0.065–0.600 V (black solid line *1*); partially blocked with CO molecules in the potential window 0.065–0.860 V (grey dashed line *2*), and first cycle after oxidative stripping of CO (black solid line *3*). The scan rate is 50 mV/s. (b) Schematic top views of the Pt(100) surface illustrating the possible restructuring of step and kink sites upon CO adsorption. The details are given in the text.

black solid curve plotted in Fig. 4 represents the first voltammetric cycle of the Pt(100)-(1 × 1) electrode in 0.5 M H_2SO_4 in 0.065 V < E < 0.600 V as recorded before CO exposure. Upon CO dosing one observes during the first 7 potential cycles a decrease of the intensity of the peak $P1$ at $E = 0.380$ V as well as of the currents below 0.150 V, whereas the peak $P2$ at 0.280 V slightly increases. Further potential cycling leads to the reduction of all features related to the adsorption of hydrogen and (bi)sulfate anions (grey traces). We also notice, that the peak $P1$, which originates from (100) terrace sites, decreases much more pronounced than the peak $P2$ around 0.280 V and the plateau region in $E < 0.200$ V, which both originate from surface defect sites. The black dashed line represents the quasi-equilibrium cycle (anodic scan before CO oxidation) between the CO sub-monolayer on Pt(100)-(1 × 1) and the bulk electrolyte. The peak $P1$ at 0.380 V almost disappeared, while the signals around $P2$ and in the potential region below 0.150 V are still relatively high. The total CO coverage θ_{CO} amounts to ~0.54 as estimated from stripping experiments (dashed line in Fig. 4) according to Eq. (5).

We may conclude that the adsorption of CO molecules at a highly ordered Pt(100)-(1 × 1) surface is favored on terraces sites. This conclusion is in agreement with the results presented in [93], where CO was adsorbed on Pt(100) electrode surface by reducing CO_2. The behavior of Pt(100) face is completely opposite to observations on stepped Pt[n(111) × (111)]. surfaces. Lebedeva et al. suggested that CO adsorbs preferentially on step sites and blocks hydrogen adsorption [11, 90]. We hypothesize that the most probable reason of this difference is the weaker adsorption of (bi)sulfate on (100) terraces as compared to structure defects (steps and kinks) on Pt(100)-(1 × 1).

Figure 5a illustrates the above interesting effect more clearly. We notice that the voltammograms in 0.065 < E < 0.600 V before CO submonolayer adsorption and after oxidative stripping coincide (curve *3* in Fig. 5a). Curve *2* represents the quasi-equilibrium CV between the CO sub-monolayer on Pt(100)-(1 × 1) and the bulk electrolyte (θ_{CO} ~ 0.18). The magnified region around $P2$ demonstrates that the adsorption of a sub-monolayer amount of CO (at least up to θ_{CO} = 0.3) leads to a current increase of $P2$. Since adsorbed CO molecules enhance the mobility of platinum adatoms, we attribute this observation to the formation of additional (111) step sites as triggered by the rearrangement of (110) steps and kinks. Figure 5b represents a schematic sketch illustrating the formation of (111) step sites by a restructuring of (110) steps (upper left) as well as of the healing of (111) steps by the transformation of positions at (111) steps (lower right). Somorjai et al. reported recently rather similar phenomena in an STM study at a solid/gas interface for a stepped Pt surface exposed to CO at pressures above 0.1 torr [94].

Figure 6 shows the results of the CO electro-oxidation current transients on Pt(100)-(1 × 1) cooled in Ar/H_2, Ar and air atmospheres for two different step potentials. The CO saturated adlayers were obtained by CO dosing at 0.150 V. The shapes of the chronoamperometric curves are rather similar: the exponentially decaying fast double layer charging segment is followed by a current plateau, and finally the main oxidation peak evolves. The plateau represents the "preignition region." The position of the main peak shifts towards longer times with decreasing overpotential of CO-oxidation. In the case of Ar and air cooling protocols the shape of the peaks is rather symmetric, which is in accordance with a Langmuir-Hinshelwood-type reaction (Eqs. (3) and (4)) between carbon monoxide and a surface oxygen-containing species [3, 14, 74, 91]. The plateaus before the main oxidation peaks are always higher for the defect-rich and less ordered sur-

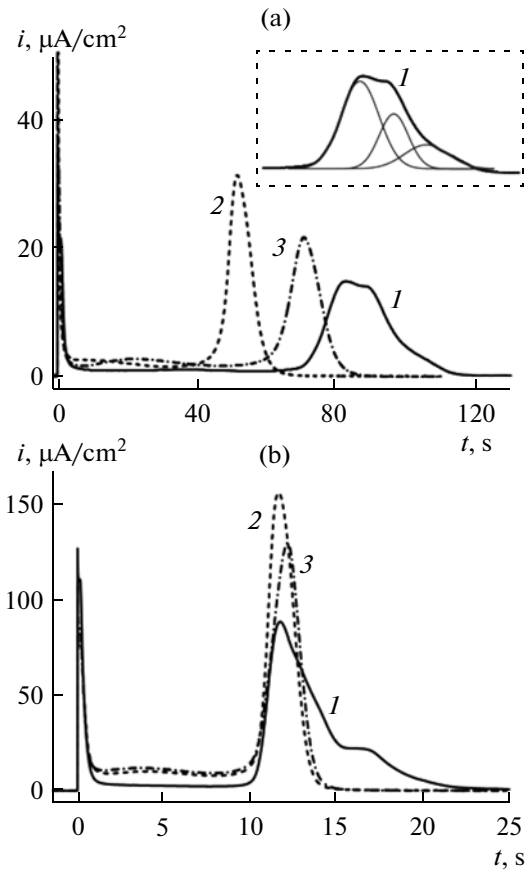

Fig. 6. CO oxidation transients recorded for a saturated CO-adlayer in CO-free 0.5 M H_2SO_4 solution at different step potentials: 0.700 V (a) and 0.750 V (b) for Pt(100) cooled in Ar/H_2 (solid lines *1*), Ar (dashed lines *2*), and air (dash-dotted lines *3*) atmospheres. CO was dosed at 0.15 V for 1 min. The inset in the panel (a) illustrates the experimental curve *1* and its deconvolution in three Gaussian-type peaks.

faces. These currents are related to CO electro-oxidation on defect sites and/or platinum ad-islands. The current plateaus preceding the main peak as well as shape and position of the latter indicate the formation of nuclei (holes) at the onset of the CO monolayer oxidation. During CO stripping the holes grow (the hole perimeter raises) and hence the current increases. After some time the holes start to overlap and the total perimeter decreases, and consequently the resulting current decreases as well.

The maxima of the recorded transients are rather broad, not symmetrical and consist of at least three contributions (see the inset in Fig. 6a) for well-ordered Pt(100) surfaces (curves *1*, Ar/H_2 cooling). We propose on basis of the above STM data that these contributions are related to the presence of different types of terraces: (1) broad terraces, (2) narrow terraces with step-bunched regions, (3) terraces with ad-islands, and (4) areas between ad-islands (Figs. 2a and 2b). The surface defects act as nucleation centers for the reaction. The oxidation of CO molecules adsorbed on broad terraces is hindered due to the slow surface diffusion of CO_{ad} to OH_{ad} species, which are preferentially adsorbed at defect sites. The CO adlayer assembles in a more closed-packed structure at wide terraces as compared to regions with a high defect density, where the structural defects disturb the long-range order of the CO layer. The CO oxidation proceeds faster in regions with higher step density. Thus, a non-uniform distribution of defect sites over the whole surface of a Pt(100) electrode as cooled in an Ar/H_2 atmosphere gives rise to a broad "multi-peak" CO-oxidation transient (Fig. 6). This explanation is supported by a theoretical study of Pethukov et al. [91], in which the authors also observed that the shape of the transient peaks broadens and appears to be less symmetric with decreasing number of structure defects. The Pt(100) electrode prepared according to Ar or air cooling protocol displays a defect-rich surface with narrow and short terraces. The distribution of defects is more regular than for the Ar/H_2-cooled electrode. Therefore, the transient peaks of CO oxidation are narrower and more symmetric (curves *2* and *3* in Fig. 6).

4. CONCLUSIONS

The cyclic voltammograms of Pt(100)-(1 × 1) electrodes cooled in different atmospheres display multiple states of hydrogen and anion adsorption. These states correlate with the nature and the density of the adsorption sites on the surface: (100) terraces, (111) and (110) steps as well as kinks. The combined voltammetric and in situ STM study demonstrates that the pretreatment of the Pt(100) electrode, in particular the cooling atmospheres, dictate the surface structure. A Pt(100) electrode cooled in a reductive Ar/H_2 atmosphere is unreconstructed and displays large ordered terraces. Terraces larger than 500 nm show arrays of regularly aligned square-shaped Pt islands. An island-free depletion zone of typically larger than 200 nm was observed near step-edges under our experimental conditions. Slightly less well-ordered Pt(100)-(1 × 1) surfaces can be prepared upon cooling in an Ar/CO atmosphere. Cooling of the annealed and reconstructed Pt(111)-(hex)*R*0.7° electrode in Ar, covering by NO and subsequent immersion into 0.5 M H_2SO_4, as well as cooling in air leads to the formation of a large number of surface defects (kinks and steps) and faceting.

The high density of structure defects on the Pt(100)-(1 × 1) plane results in a higher activity towards CO electro-oxidation. However, the effect of defect sites on the oxidative CO stripping is not as dramatic as reported for Pt(111) [90]. The reaction of CO oxidation is qualitatively described by a Langmuir-Hinshelwood mechanism and controlled by a nucleation and growth process. An increase of the magnitude of the peak *P*2 at 0.280 V was observed in the corresponding cyclic voltammogram at low submonolayer CO coverages ($\theta < 0.3$), which could be attributed to a rearrangement of (110) steps and/or kinks into (111) steps as the result of a mobility enhancement of platinum ad-atoms by adsorbed CO

molecules. We demonstrated also that the adsorption of CO molecules on the Pt(100)-(1 × 1) surface occurs preferentially at (100) terrace sites due to the blocking of defect sites (steps and kinks) by specifically adsorbed (bi)sulfate anions. A rather small amount of structure defects and the high irregularity of their distribution over the whole Pt(100) electrode surface (cooled in an Ar/H_2 atmosphere) give rise to broad multiple-peak transient features of CO oxidation.

The current experimental observations and their tentative interpretations represent a first step towards developing an atomic-level picture on the role of surface structure in the CO electro-oxidation on electrified Pt(100)-(1 × 1) electrodes in contact with 0.5 M H_2SO_4. Complementary attempts to model the experimental results employing multi-scale DFT calculations are underway.

ACKNOWLEDGMENTS

This research was supported by the University of Bern (Switzerland), the A.N. Frumkin Institute of Physical Chemistry and Electrochemistry (Moscow, Russia), CEST and the Swiss National Science Foundation.

REFERENCES

1. Markovic, N.M. and Ross, P.N., *Surf. Sci. Rep.*, 2002, vol. 45, p. 117.
2. Spendelow, J.S. and Wieckowski, A., *Phys. Chem. Chem. Phys.*, 2004, vol. 6, p. 5094.
3. Xu, Q., Linke, U., Bujak, R., and Wandlowski, T., *Electrochim. Acta*, 2009, vol. 54, p. 5509.
4. Adzic, R.R., Tripkovic, A.V., and Markovic, N.M., *J. Electroanal. Chem.*, 1983, vol. 150, p. 79.
5. Tian, N., Zhou, Z.-Y., and Sun, S.-G., *J. Phys. Chem., Ser. C*, 2008, vol. 112, p. 19801.
6. Stamenkovic, V., Mun, B.S., Mayrhofer, K.J.J., Ross, P.N., Markovic, N.M., Rossmeisl, J., Greeley, J., and Nørskov, J.K., *Angew. Chem. Int. Ed.*, 2006, vol. 45, p. 2897.
7. Besenbacher, F., Chorkendorff, I., Clausen, B.S., Hammer, B., Molenbroek, A.M., Nørskov, J.K., and Stensgaard, I., *Science*, 1998, vol. 279, p. 1913.
8. Koper, M.T.M., Ed., *Fuel Cell Catalysis: a Surface Science Approach*, Hoboken: Wiley, 2009.
9. Spendelow, J.S. and Wieckowski, A., *Phys. Chem. Chem. Phys.*, 2007, vol. 9, p. 2654.
10. Stamenkovic, V.R., Mun, B.S., Arenz, M., Mayrhofer, K.J.J., Lucas, C.A., Wang, G., Ross, P.N., and Markovic, N.M., *Nat. Mater.*, 2007, vol. 6, p. 241.
11. Lebedeva, N.P., Koper, M.T.M., Herrero, E., Feliu, J.M., and van Santen, R.A., *J. Electroanal. Chem.*, 2000, vol. 487, p. 37.
12. Markovic, N.M., Lucas, C.A., Rodes, A., Stamenkovic, V., and Ross, P.N., *Surf. Sci.*, 2002, vol. 499, p. L149.
13. Spendelow, J.S., Goodpaster, J.D., Kenis, P.J.A., and Wieckowski, A., *J. Phys. Chem., Ser. B*, 2006, vol. 110, p. 9545.
14. Inkaew, P., Zhou, W., and Korzeniewski, C., *J. Electroanal. Chem.*, 2008, vol. 614, p. 93.
15. Samjeske, G., Miki, A., Ye, S., and Osawa, M., *J. Phys. Chem., Ser. B*, 2006, vol. 110, p. 16559.
16. Grozovski, V., Climent, V., Herrero, E., and Feliu, J.M., *Chem. Phys. Chem.*, 2009, vol. 10, p. 1922.
17. Taguchi, S. and Feliu, J.M., *Electrochim. Acta*, 2007, vol. 52, p. 6023.
18. Dima, G.E., Beltramo, G.L., and Koper, M.T.M., *Electrochim. Acta*, 2005, vol. 50, p. 4318.
19. Molodkina, E.B., Ehrenburg, M.R., Polukarov, Y.M., Danilov, A.I., Souza-Garcia, J., and Feliu, J.M., *Electrochim. Acta*, 2010, vol. 56, p. 154.
20. Solla-Gullon, J., Rodriguez, P., Herrero, E., Aldaz, A., and Feliu, J.M., *Phys. Chem. Chem. Phys.*, 2008, vol. 10, p. 1359.
21. Rudnev, A.V., Molodkina, E.B., Danilov, A.I., Polukarov, Y.M., Berna, A., and Feliu, J.M., *Electrochim. Acta*, 2009, vol. 54, p. 3692.
22. Danilov, A.I., Molodkina, E.B., Rudnev, A.V., Polukarov, Y.M., and Feliu, J.M., *Electrochim. Acta*, 2005, vol. 50, p. 5032.
23. Danilov, A.I., Nazmutdinov, R.R., Zinkicheva, T.T., Molodkina, E.B., Rudnev, A.V., Polukarov, Y.M., and Feliu, J.M., *Russ. J. Electrochem.,* 2008, vol. 44, p. 697.
24. Herrero, E., Buller, L.J., and Abruna, H.D., *Chem. Rev.*, 2001, vol. 101, p. 1897.
25. Thiel, K.O., Hintze, M., Vollmer, A., and Donner, C., *J. Electroanal. Chem.*, 2008, vol. 621, p. 7.
26. Yokoyama, M., Liang, W.S., Chen, W., Wee, A.T.S., Matsui, T., and Yuhara, J., *Surf. Sci.*, 2011, vol. 605, p. 844.
27. Okada, J., Inukai, J., and Itaya, K., *Phys. Chem. Chem. Phys.*, 2001, vol. 3, p. 3297.
28. Francke, R., Climent, V., Baltruschat, H., and Feliu, J.M., *J. Electroanal. Chem.*, 2008, vol. 624, p. 228.
29. Kolb, D.M., in *Advances in Electrochemical Science and Engineering*, Alkire, R.C. and Kolb, D.M., Eds., Weinheim: Wiley-VCH, 2001, vol. 7, p. 107.
30. Domke, K.F., Xiao, X.-Y., and Baltruschat, H., *Electrochim. Acta*, 2009, vol. 54, p. 4829.
31. Hazzazi, O.A., Attard, G.A., Wells, P.B., Vidal-Iglesias, F.J., and Casadesus, M., *J. Electroanal. Chem.*, 2009, vol. 625, p. 123.
32. Strmcnik, D.S., Tripkovic, D.V., van der Vliet, D., Chang, K.-C., Komanicky, V., You, H., Karapetrov, G., Greeley, J.P., Stamenkovic, V.R., and Markovic, N.M., *J. Am. Chem. Soc.*, 2008, vol. 130, p. 15332.
33. Karlberg, G.S., Jaramillo, T.F., Skulason, E., Rossmeisl, J., Bligaard, T., and Norskov, J.K., *Phys. Rev. Lett.*, 2007, vol. 99, p. 126101.
34. Nørskov, J.K., Abild-Pedersen, F., Studt, F., and Bligaard, T., *Proc. Natl Acad. Sci.*, 2011, vol. 108, p. 937.
35. Shingaya, Y., Matsumoto, H., Ogasawara, H., and Ito, M., *Surf. Sci.*, 1995, vol. 335, p. 23.
36. Furuya, N. and Shibata, M., *J. Electroanal. Chem.*, 1999, vol. 467, p. 85.
37. Kibler, L.A., Cuesta, A., Kleinert, M., and Kolb, D.M., *J. Electroanal. Chem.*, 2000, vol. 484, p. 73.
38. Itaya, K., *Prog. Surf. Sci.*, 1998, vol. 58, p. 121.
39. Clavilier, J., *J. Electroanal. Chem.*, 1980, vol. 107, p. 211.

40. Clavilier, J., Faure, R., Guinet, G., and Durand, R., *J. Electroanal. Chem.*, 1980, vol. 107, p. 205.
41. Clavilier, J., Durand, R., Guinet, G., and Faure, R., *J. Electroanal. Chem.*, 1981, vol. 127, p. 281.
42. Clavilier, J., Armand, D., and Wu, B.L., *J. Electroanal. Chem.*, 1982, vol. 135, p. 159.
43. Clavilier, J. and Armand, D., *J. Electroanal. Chem.*, 1986, vol. 199, p. 187.
44. Scortichini, C.L. and Reilley, C.N., *J. Electroanal. Chem.*, 1982, vol. 139, p. 233.
45. Scortichini, C.L., Woodward, F.E., and Reilley, C.N., *Electroanal. Chem.*, 1982, vol. 139, p. 265.
46. Clavilier, J., in *Interfaciai Electrochemistry: Theory, Experimental, and Applications*, Wieckowski, A., Ed., New York: Marcel Dekker, 1999, p. 231.
47. Climent, V., Gomez, R., Orts, J.M., Rodes, A., Aldaz, A., and Feliu, J.M., in *Interfacial Electrochemistry*, Wieckowski, A., Ed., New York: Marcel Dekker, Inc., 1999, p. 463.
48. Hubbard, A.T., Ishikawa, R.M., and Katekaru, J., *J. Electroanal. Chem. Interfacial Electrochem.*, 1978, vol. 86, p. 271.
49. Wagner, F.T. and Ross P.N., Jr., *J. Electroanal. Chem. Interfacial Electrochem.*, 1983, vol. 150, p. 141.
50. Heilmann, P., Heinz, K., and Müller, K., *Surf. Sci.*, 1979, vol. 83, p. 487.
51. Thiel, P.A., Behm, R.J., Norton, P.R., and Ertl, G., *Surf. Sci.*, 1982, vol. 121, p. L553.
52. Behm, R.J., Thiel, P.A., Norton, P.R., and Ertl, G., *J. Chem. Phys.*, 1983, vol. 78, p. 7437.
53. Cox, M.P., Ertl, G., Imbihl, R., and Rustig, J., *Surf. Sci.*, 1983, vol. 134, p. L517.
54. Thiel, P.A., Behm, R.J., Norton, P.R., and Ertl, G., *J. Chem. Phys.*, 1983, vol. 78, p. 7448.
55. Motoo, S. and Furuya, N., *J. Electroanal. Chem. Interfaciai Electrochem.*, 1984, vol. 172, p. 339.
56. Motoo, S. and Furuya, N., *Ber. Bunsen-Ges. Phys. Chem.*, 1987, vol. 91, p. 457.
57. Markovic, N.M., Marinkovic, N.S., and Adzic, R.R., *J. Electroanal. Chem.*, 1988, vol. 241, p. 309.
58. Palaikis, L., Zurawski, D., Hourani, M., and Wieckowski, A., *Surf. Sci.*, 1988, vol. 199, p. 183.
59. Al-Akl, A., Attard, G.A., Price, R., and Timothy, B., *J. Electroanal. Chem.*, 1999, vol. 467, p. 60.
60. Wakisaka, M., Sugimasa, M., Inukai, J., and Itaya, K., *J. Electrochem. Soc.*, 2003, vol. 150, p. E81.
61. Clavilier, J., Orts, J.M., and Feliu, J.M., *J. Phys., Ser. IV,* 1994, vol. 4, p. 303.
62. Feliu, J.M., Rodes, A., Orts, J.M., and Clavilier, J., *Pol. J. Chem.*, 1994, vol. 68, p. 1575.
63. Clavilier, J., Armand, D., Sun, S.G., and Petit, M., *J. Electroanal. Chem.*, 1986, vol. 205, p. 267.
64. Hara, M., Linke, U., and Wandlowski, T., *Electrochim. Acta*, 2007, vol. 52, p. 5733.
65. Rodes, A., Climent, V., Orts, J.M., Pérez, J.M., and Aldaz, A., *Electrochim. Acta*, 1998, vol. 44, p. 1077.
66. Horcas, I., Fernandez, R., Gomez-Rodriguez, J.M., Colchero, J., Gomez-Herrero, J., and Baro, A.M., *Rev. Sci. Instrum.,* 2007, vol. 78, p. 013705.
67. Armand, D. and Clavilier, J., *J. Electroanal. Chem.*, 1987, vol. 225, p. 205.
68. Armand, D. and Clavilier, J., *J. Electroanal. Chem.*, 1987, vol. 233, p. 251.
69. Rodes, A., Zamakhchari, M.A., Elachi, K., and Clavilier, J., *J. Electroanal. Chem.*, 1991, vol. 305, p. 115.
70. Watanabe, S., Inukai, J., and Ito, M., *Surf. Sci.*, 1993, vol. 293, p. 1.
71. Vidal-Iglesias, F.J., Solla-Gullón, J., Campica, J.M., Herrero, E., Aldaz, A., and Feliu, J.M., *Electrochim. Acta*, 2009, vol. 54, p. 4459.
72. Garcia-Araez, N., Climent, V., Herrero, E., and Feliu, J.M., *Surf. Sci.*, 2004, vol. 560, p. 269.
73. Clavilier, J., Rodes, A., Elachi, K., and Zamakhchari, M.A., *J. Chim. Phys.-Chim. Biol.*, 1991, vol. 88, p. 1291.
74. Markovic, N.M., Lucas, C.A., Grgur, B.N., and Ross, P.N., *J. Phys. Chem., Ser. B*, 1999, vol. 103, p. 9616.
75. Sashikata, K., Sugata, T., Sugimasa, M., and Itaya, K., *Langmuir*, 1998, vol. 14, p. 2896.
76. Pennemann, B., Oster, K., and Wandelt, K., *Surf. Sci.*, 1991, vol. 249, p. 35.
77. Norton, P.R., Creber, D.K., and Davies, J.A., *J. Vac. Sci. Technol.*, 1980, vol. 17, p. 149.
78. Horch, S., Lorensen, H.T., Helveg, S., Laegsgaard, E., Stensgaard, I., Jacobsen, K.W., Norskov, J.K., and Besenbacher, F., *Nature*, 1999, vol. 398, p. 134.
79. Zei, M.S., Batina, N., and Kolb, D.M., *Surf. Sci.*, 1994, vol. 306, p. L519.
80. Al-Akl, A., Attard, G., Price, R., and Timothy, B., *Phys. Chem. Chem. Phys.*, 2001, vol. 3, p. 3261.
81. Wu, K. and Zei, M.S., *Surf. Sci.*, 1998, vol. 415, p. 212.
82. Gómez, R., Feliu, J.M., Aldaz, A., and Weaver, M.J., *Surf. Sci.*, 1998, vol. 410, p. 48.
83. Domke, K., Herrero, E., Rodes, A., and Feliu, J.M., *J. Electroanal. Chem.*, 2003, vol. 552, p. 115.
84. López-Cudero, A., Cuesta, A., and Gutiérrez, C., *J. Electroanal. Chem.*, 2006, vol. 586, p. 204.
85. Lucas, C.A., Markovic, N.M., and Ross, P.N., *Surf. Sci.*, 1999, vol. 425, p. L381.
86. Markovic, N.M., Grgur, B.N., Lucas, C.A., and Ross, P.N., *J. Phys. Chem., Ser. B,* 1999, vol. 103, p. 487.
87. Gilman, S., *J. Phys. Chem.*, 1964, vol. 68, p. 70.
88. Lebedeva, N.P., Rodes, A., Feliu, J.M., Koper, M.T.M., and van Santen, R.A., *J. Phys. Chem., Ser. B*, 2002, vol. 106, p. 9863.
89. Koper, M.T.M., Lebedeva, N.P., and Hermse, C.G.M., *Faraday Discuss.*, 2002, vol. 121, p. 301.
90. Lebedeva, N.P., Koper, M.T.M., Feliu, J.M., and van Santen, R.A., *Electrochem. Commun.*, 2000, vol. 2, p. 487.
91. Petukhov, A.V., Akemann, W., Friedrich, K.A., and Stimming, U., *Surf. Sci.*, 1998, vols. 402–404, p. 182.
92. López-Cudero, A., Cuesta, A., and Gutiérrez, C., *J. Electroanal. Chem.*, 2003, vol. 548, p. 109.
93. Rodes, A., Pastor, E., and Iwasita, T., *J. Electroanal. Chem.*, 1994, vol. 377, p. 215.
94. Tao, F., Dag, S., Wang, L.-W., Liu, Z., Butcher, D.R., Bluhm, H., Salmeron, M., and Somorjai, G.A., *Science*, 2010, vol. 327, p. 850.